Observation of the $J \leqslant 7/2$ low-spin states in ^{213}Fr populated in the electron capture of the $1/2^-$ ground state of ^{213}Ra

C. Clisu,[1,2] A. N. Andreyev,[3,4] C. R. Nita,[1,*] R. Lica,[1,5] H. Naïdja,[6] B. Andel,[7] S. Antalic,[7] T. A. Berry,[8] M. J. G. Borge,[5,9] T. E. Cocolios,[10] C. Costache,[1] J. G. Cubiss,[3,5] H. De Witte,[10] L. M. Fraile,[11] H. Fynbo,[12] V. M. Gadelshin,[13] C. Granados,[5] P. Greenlees,[14,15] R. Heinke,[13] M. Huyse,[10] I. Lazarus,[12] D. Leimbach,[5,13,16] N. Marginean,[1] R. Marginean,[1] B. A. Marsh,[5] C. Mihai,[1] P. Mosat,[7] E. Nacher,[17] A. Negret,[1] J. D. Ovejas,[9] R. D. Page,[18] S. Pascu,[1] A. Perea,[9] Zs. Podolyak,[8] V. Pucknell,[19] P. Rahkila,[14,15] K. Rezynkina,[10] R. E. Rossel,[5] C. O. Sotty,[1] L. Stan,[1,2] D. Studer,[13] O. Tengblad,[9] P. Van Duppen,[10] V. Vedia,[11] and N. Warr[20]
(The IDS Collaboration)

[1]*Horia Hulubei National Institute for Physics and Nuclear Engineering, RO-077125 Bucharest, Romania*
[2]*Department of Physics, University Politehnica of Bucharest, Splaiul Independentei 313, 060042 Bucharest, Romania*
[3]*School of Physics, Engineering and Technology, University of York, YO10 5DD, York, United Kingdom*
[4]*Advanced Science Research Center, Japan Atomic Energy Agency, Tokai-mura, Japan*
[5]*ISOLDE, CERN, CH-1211 Geneva 23, Switzerland*
[6]*Université Constantine 1, Laboratoire de Physique Mathématique et Subatomique (LPMPS), 1 Route Ain El Bey, 25000 Constantine, Algeria*
[7]*Department of Nuclear Physics and Biophysics, Comenius University in Bratislava, 84248 Bratislava, Slovakia*
[8]*Department of Physics, University of Surrey, Guildford GU2 7XH, United Kingdom*
[9]*Instituto de Estructura de la Materia, CSIC, Serrano 113 bis, E-28006 Madrid, Spain*
[10]*KU Leuven, Instituut voor Kern- en Stralingsfysica, Celestijnenlaan 200D, 3001 Leuven, Belgium*
[11]*Grupo de Física Nuclear EMFTEL & IPARCOS, Universidad Complutense de Madrid, 28040, Madrid, Spain*
[12]*Department of Physics and Astronomy, Aarhus University, DK-8000 Aarhus C, Denmark*
[13]*Johannes Gutenberg-University, Saarstraße 21, 55122 Mainz, Germania*
[14]*University of Jyvaskyla, Department of Physics, Accelerator Laboratory, P.O. Box 35(YFL), FI-40014 University of Jyvaskyla, Finland*
[15]*Helsinki Institute of Physics, University of Helsinki, P.O. Box 64, FI-00014 Helsinki, Finland*
[16]*Department of Physics, University of Gothenburg, Origovägen 6 B, 41296 Göteborg, Sweden*
[17]*Instituto de Fisica Corpuscular, CSIC - Universidad de Valencia, E-46980, Valencia, Spain*
[18]*Department of Physics, Oliver Lodge Laboratory, University of Liverpool, Liverpool L69 7ZE, United Kingdom*
[19]*STFC Daresbury, Daresbury, Warrington WA4 4AD, United Kingdom*
[20]*Institut für Kernphysik, Universität zu Köln, 50937 Köln, Germany*

(Received 1 August 2024; accepted 26 November 2024; published 16 December 2024)

A detailed level scheme of $^{213}Fr_{126}$ following the EC/β^+ decay of the $1/2^-$ ^{213}Ra parent ground state was built in an experiment performed at the ISOLDE Decay Station, CERN. The fragmented total β decay strength favours the direct population of several low-spin ($J \leqslant 7/2$) excited states. The analysis of the γ-singles spectrum and γ-γ coincidences allowed us to identify many new γ-ray transitions and excited states in ^{213}Fr up to about 3.6 MeV excitation energy. The spins and parities of the newly established levels, on top of the $(7/2^-_1)$ state, were mainly assigned based on the systematics of the $N = 126$ isotones and further compared with shell-model calculations. The level scheme displays a structural pattern, with several groups of states with negative parity, emerging from the well-defined, simple, $\pi(h^5_{9/2})$, $\pi(h^4_{9/2}f^1_{7/2})$ configurations or from their configuration mixing. The strength of the $E2$ transitions within the multiplets is compared with shell-model theoretical calculations performed with the *KHPE* and *H*208 effective interactions. A new $(3/2^-)$ isomer with a half-life of 26(3) ns has been identified. An upper limit of 35 ps was determined for the half-life of the first excited state, $7/2^-$. The possibility of a mixed $M1$+$E2$ character is discussed for the $7/2^-_1 \rightarrow 9/2^-_{gs}$ decay in ^{213}Fr, which leads to an l-forbidden nature of the $\pi f_{7/2} \rightarrow \pi h_{9/2}$ transition.

DOI: 10.1103/PhysRevC.110.064315

*Contact author: cristina.nita@nipne.ro

Published by the American Physical Society under the terms of the Creative Commons Attribution 4.0 International license. Further distribution of this work must maintain attribution to the author(s) and the published article's title, journal citation, and DOI. Open access publication funded by CERN.

I. INTRODUCTION

Nuclei in the proximity of shell closures are of interest since they represent a benchmark test for the shell-model calculations. These nuclei are of particular significance as they may provide insight into the role and manifestations of core polarization, pairing [1], and other types of residual interactions, such as the quadrupole interaction.

With exactly $N = 126$ neutrons and lying in the vicinity of $Z = 82$, the low-energy excited states of ^{213}Fr ($Z = 87$) are expected to be dominated by spherical $j^5 = (h^5_{9/2})_{J^-}$ proton configurations. Simple configurations were proposed for the $9/2^-_{gs}$, the $7/2^-_1$, and the $13/2^+$ states in the odd-A, $N = 126$ isotones [1–6] as $\pi h^n_{9/2}$, $\pi f^1_{7/2}$ and $\pi i^1_{13/2}$, respectively, where n are the extra protons above $Z = 82$. The ground-state spin was determined by Coc *et al.* [7] to be $9/2^-$. The first two excited states, at 498 and 1105 keV, respectively, were observed in an α-decay study of the $29/2^+$ isomer in ^{217}At performed by Decman *et al.* [8]. They were tentatively assigned as $J^\pi = (7/2^-)$ and $(13/2)^+$ based on the conversion coefficients of their corresponding transitions to the ground state.

The spectroscopic information concerning the low-spin states is quite scarce. It can be accessed via β-decay spectroscopy of the $J^\pi = 1/2^-$ ground state of ^{213}Ra [$T_{1/2} = 2.73(5)$ min.] [9], which has a 13(2)% electron capture (EC) + β^+ decay branch to ^{213}Fr [10]. Information on the low-J states of ^{213}Fr was originally reported by Maier [11] by combining the results obtained from the α decay of ^{217}Ac and the EC decay of ^{213}Ra. Their obtained level scheme includes four excited states arranged in a $9/2^-_{gs}$–$7/2^-_1$–$(7/2^-_2)$–$(5/2^-_1)$–$(3/2^-_1)$ sequence up to an energy of 1170 keV. The ^{213}Ra EC decay was also observed by Guttormsen *et al.* [12] where conversion electrons were detected with a superconducting electron detection system in coincidence with the francium K_α lines. They assigned the 175-, 195-, 208-, 218-, 227-, 257-, 317-, 339-, 400-, 475-, and 498-keV transitions to ^{213}Fr. A second measurement performed by Pragati *et al.* [13] using a MINI-ORANGE spectrometer coupled with two HPGe detectors, identified the corresponding 399.7-, 498.0-, and 520.4-keV γ rays from ^{213}Fr. Neither experiment presents any information on their decay pattern, intensity values, or internal conversion coefficients (IC).

Additionally, the $7/2^-_1 \rightarrow 9/2^-_{gs}$ transitions in ^{209}Bi and ^{211}At were deduced to have $M1{+}E2$ mixing ratios of $\delta = -0.62(6)$ [2,14] and $-0.65(6)$ [15], respectively. It results that the $M1$ component accounts for $1/(1+\delta^2) \approx 70\%$ of the total strength. This transition must then have a sizable l-forbidden $M1$ character component since it breaks the rule of $\Delta l = 0$. It was observed experimentally that the single-particle orbits in the vicinity of major shell gaps having $(n, l, j = l + 1/2)$ and $(n-1, l+2, j = l + 3/2)$ quantum numbers develop a near degeneracy [16,17]. Several neutron transitions have been investigated nearby ^{208}Pb [18] between $h_{9/2} \leftrightarrow f_{7/2}$, $g_{7/2} \leftrightarrow d_{5/2}$, $f_{5/2} \leftrightarrow p_{3/2}$ and $d_{3/2} \leftrightarrow s_{1/2}$ orbits. An l-forbidden $d_{5/2} \rightarrow g_{7/2}$ $M1$ transition has also been found at lower masses, nearby $Z = 50$ and $N = 82$, in ^{129}Sn [19]. In ^{213}Fr, the proton $h_{9/2}$ and $f_{7/2}$ orbits might be pseudospin partners and form a doublet. Given the encountered similarities with the $N = 126$ isotones it is expected that this hidden symmetry could also be displayed in ^{213}Fr.

We report here on a detailed γ-ray spectroscopy study of ^{213}Fr, populated in the EC/β^+ decay of ^{213}Ra, produced at the ISOLDE facility. Section II contains the beam conditions and the experimental setup used in two separate runs. The first run was dedicated to a detailed spectroscopic study of ^{213}Fr while the aim of the second run was to measure the half-life of the $7/2^-_1$ excited state through the fast electronic timing technique. The γ-ray spectroscopy of ^{213}Fr is presented in Sec. III A, the experimental log ft values for the EC/β^+ decay branches are presented in Sec. III B, the half-life measurements for the 1170-keV and the 498-keV excited states are presented in Secs. III C and III D, respectively. Section IV comprises two independent spherical shell-model descriptions of ^{213}Fr within the j-j coupling scheme by using the KHPE and $H208$ effective interactions developed for a specific model space. Section V contains the interpretation of the experimental data integrating the theoretical description.

II. EXPERIMENTAL SETUP

The experiment was performed at the ISOLDE facility at CERN. A 1.4-GeV proton beam delivered by the PS-Booster was impinged on a 46 g/cm^2 UC_x target, inducing through spallation reactions the production of ^{213}Ra and its isobar ^{213}Fr. In order to separate the strongly produced ^{213}Fr contamination, CF_4 gas was added to the target unit, maintained at a high temperature (≈2000 °C), allowing the formation and extraction of the ^{213}Ra $^{19}F^+$ molecular ions. They were subsequently extracted from the target unit. The General Purpose Separator (GPS) setting of $A = 232$ led to the removal of the ^{213}Fr contamination as it does not produce stable molecular fluoride ions. The radioactive beam was transported to the ISOLDE Decay Station (IDS) [20,21], where it was implanted on an aluminized Mylar tape.

In the first run, the IDS consisted of four high-efficiency HPGe clover detectors positioned upstream with respect to the beam direction. Two detectors were equipped with a thin carbon epoxy window to detect low-energy x rays and γ rays down to about 30 keV. The energy calibration was performed with a ^{152}Eu standard spectroscopic source and extended up to 3 MeV by using the 1460.8- (^{40}K), 1764.5- (^{214}Bi), 2204.2- (^{214}Bi), and 2614.5-keV (^{208}Tl) natural background γ rays. The array has 2.77(2) keV energy resolution and 3.30(7)% absolute detection efficiency measured for the 1408-keV transition in ^{152}Eu.

In the second run, a pair of conical 1.5 × 1.5 × 1.0" $LaBr_3$(Ce) scintillation detectors, separated by 180°, was added to the experimental setup. The characteristic energy and time resolutions were measured by using the coincident 463–1436-keV γ rays following the β^- decay of ^{138}Cs implanted on the tape. The individual energy resolutions of the $LaBr_3$(Ce) detectors were found to be 20.3(1) and 23.4(1) keV, respectively, at 463 keV. The time differences between the fast scintillators were measured by means of time-to-amplitude-converter (TAC) modules with a 50 ns range. The obtained time distribution for the subpicosecond ($T_{1/2} < 1$ ps) [22] 2^+_1 state gave a resolution measured as FWHM of

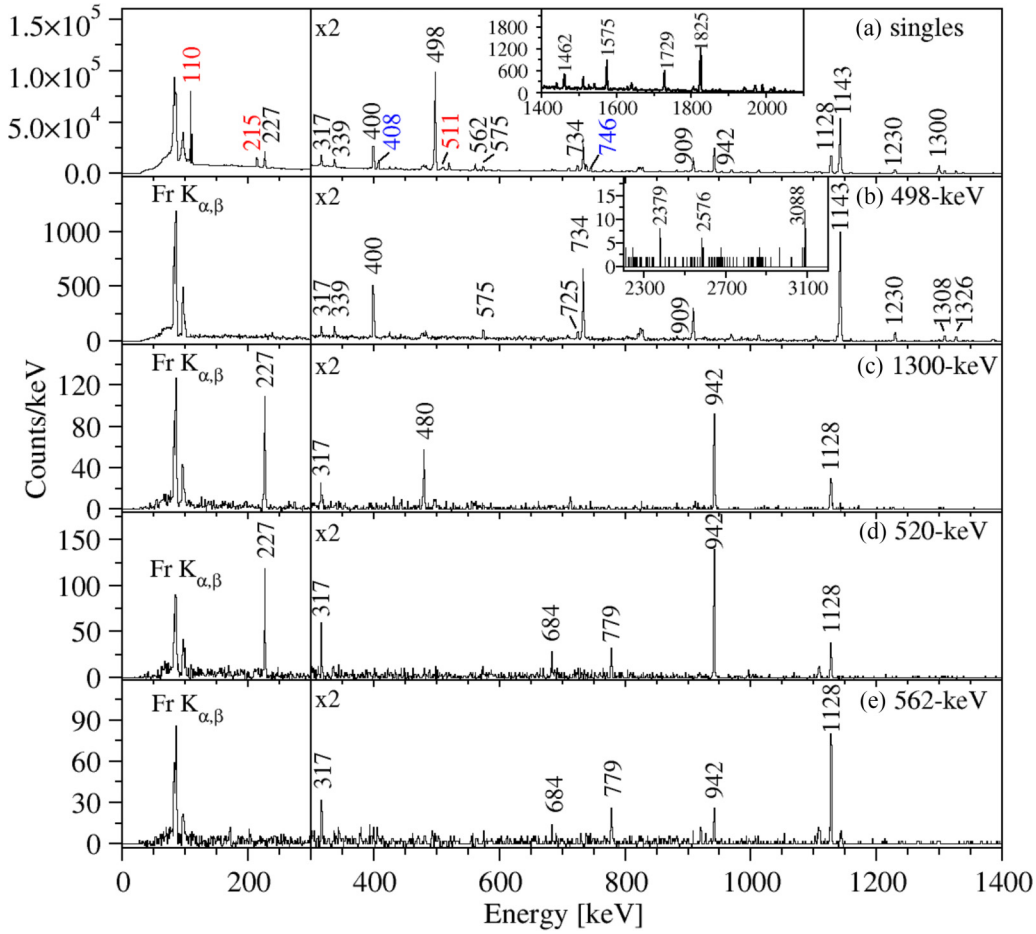

FIG. 1. (a) Singles energy spectrum obtained in the α and EC decay of ^{213}Ra, where the ^{213}Fr transitions are labeled in black, ^{209}Rn in red and ^{209}At in blue. The coincidence spectra gated with a particular γ ray are presented in (b) gate: 498 keV; (c) gate: 1300 keV; (d) gate: 521 keV; (e) gate: 562 keV. Inset to panel (a) The high-energy transitions seen in the singles spectrum extended up to 2200 keV. Inset to panel (b) The high-energy γ-ray transitions directly feeding the 498-keV state. The 2576-keV peak is coincident with 498- and 511-keV and represents the single escape peak of the 3088-keV transition. The (c), (d), and (e) gates show the statistics acquired in: the (942 $\rightarrow$ 0 keV) 942-keV transition, the statistics in the 942-keV doublet and the (2632 $\rightarrow$ 1690 keV) 942-keV transition, respectively.

231(5) ps. To correct any slight nonlinearity of the integration over the intensity range, a standard time calibrator was employed. The minimization of the energy dependence of the time response induced by the CFD modules was achieved by using implanted ^{138}Cs.

Both data sets were acquired in triggerless list mode with the NUTAQ digital acquisition system and a 100-MHz sampling time, operated using the MIDAS control program. Subsequently, the events were built using the GASPWARE analysis framework within a coincidence gate of 0.8 µs for the first run and 1 µs for the second run, allowing the data to be sorted into symmetric γ-γ matrices and also $E_{\gamma,\text{Start}}$–$E_{\gamma,\text{Stop}}$–ΔT cubes for the $LaBr_3$(Ce) detectors.

III. DATA ANALYSIS

A. γ-ray spectroscopy

In the first run, the continuous ^{213}Ra ^{19}F beam was implanted on the tape, which was moved every 20 s to reduce the contribution from the ^{209}Rn decay ($T_{1/2} = 28.5(10)$ min [23]). The absolute γ intensity of the 110-keV transition from ^{209}Rn [23] was used to estimate the total of $1.3(2) \times 10^7$ ^{213}Ra nuclei decayed in a measurement time of 214 s. The singles γ-ray spectrum presented in Fig. 1(a) is dominated by the ^{213}Ra decay products thus confirming the beam purity.

A detailed level scheme was built based on the γ-γ analysis and the prior knowledge of the 498-keV, $(7/2^-_1) \rightarrow 9/2^-_{gs}$, transition. The characteristic Fr x rays were used to distinguish between the ^{213}Fr transitions from the EC/β^+ decay of ^{213}Ra and other decay products. Figure 1(b) shows the energy spectrum gated on the 498-keV transition where the characteristic $K_{\alpha,\beta}$ lines of francium, together with a multitude of new γ rays can be seen. The newly established level scheme was extended with 17 new excited states and 35 new transitions as presented in Fig. 2. Three γ rays with $I_\gamma < 0.1$ were only tentatively placed in the level scheme. Generally, the summing effects for coincident γ rays were found to be negligible. The contribution for the intense 498–1142-keV pair of transitions gives $\approx$0.5% and raises up to $\approx$1.5–3 % when considering the coincidence between the intense low-energy transitions with

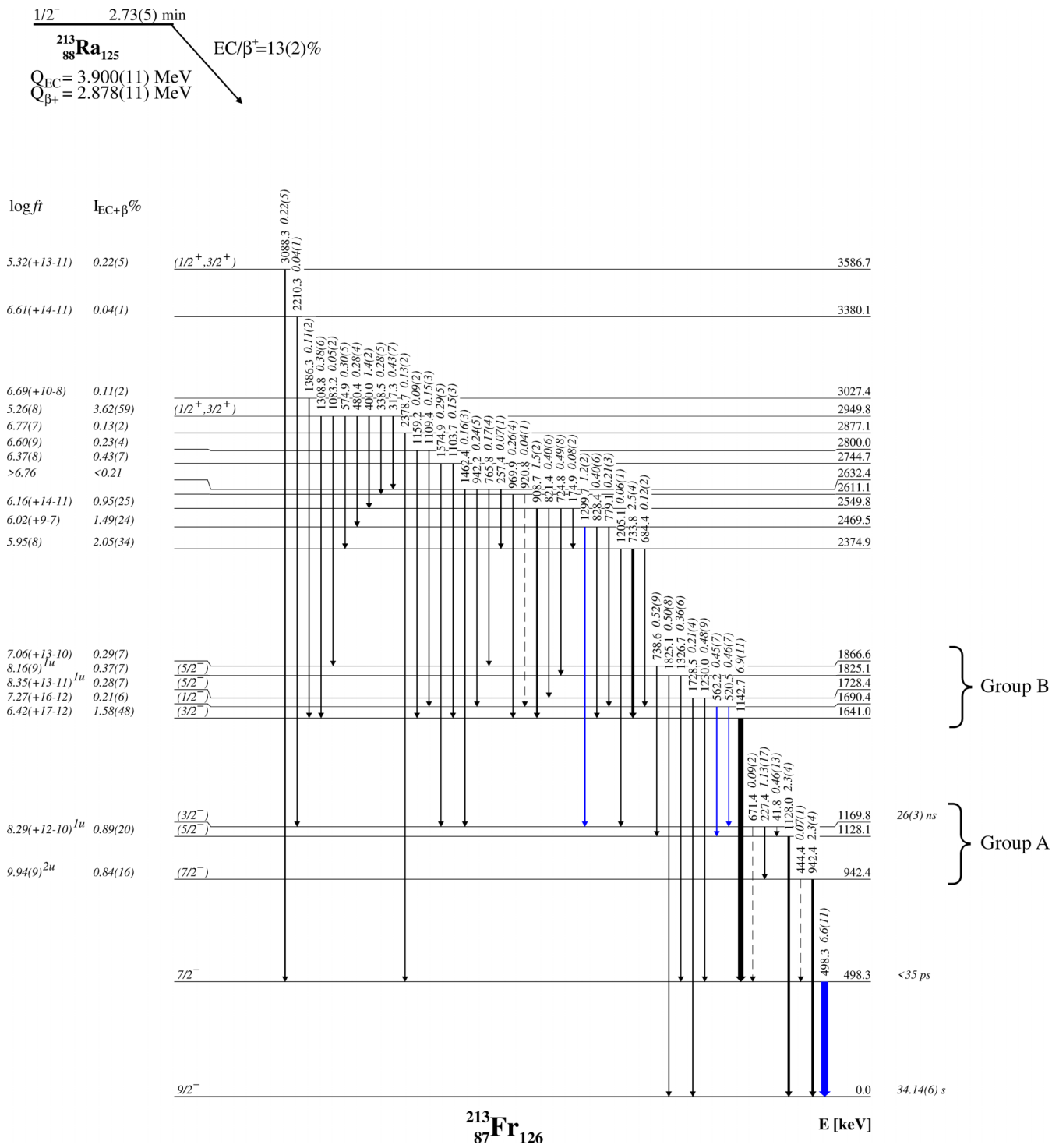

FIG. 2. The experimental level scheme of ^{213}Fr obtained from ^{213}Ra ground state EC/β^+ decay, extended on top of the previously known $7/2^-_1$ state. The Q_{EC}, Q_{β^+} and the ground state half-life are the evaluated values taken from Refs. [27] and [28], respectively. The EC branching ratio is the revised value given by Lorenz *et al.* [10]. The gating transitions from Fig. 1 are presented in blue. The transitions with dashed line are tentative. The log ft and β feeding values, the 1170-keV and the 498-keV state half-lives were obtained in this work, see Secs. III B–III D for details. The log ft values calculation and the *1u, 2u* indices are detailed in Sec. III B. The energies of the states were obtained by performing a global minimization with GTOL [26]. The I_γ labels represent absolute values (see Table I). For the Group A and Group B bands intrinsic structure please see the text and Fig. 6.

the characteristic Fr x rays. The area of the identified summing peaks was used to correct the absolute intensities. The $E_\gamma <$ 600 keV transitions were assumed to have $E/M\ \Delta L = 1, 2$ multipolarity. For the states from Group A and Group B, see Fig. 2, only $M1$, $E2$ multipolarities were considered. For the transitions observed in the conversion electron spectra from Ref. [12,13], the $E1$ multipolarity was excluded due to a very low conversion coefficient [of $\alpha(E1) = 10^{-1}$–10^{-2} for $E_\gamma < 600$ keV], see Table I.

Our work confirmed the ^{213}Fr level scheme reported by Maier [11] and placed the 175-, 317-, 339-, 400-, and 520-keV transitions assigned to ^{213}Fr by Guttormsen *et al.* [12] and Pragati *et al.* [13]. The 195-keV, 208-keV, and 218-keV transitions reported by Guttormsen *et al.* in their Fig. 11 [12], with CE_K energies of 94, 106, and 116 keV, have not been observed in this work. A possible explanation resides in the fact that ^{213}Ra decays via two competing processes, 87(2)%(α) ^{209}Rn and 13(2)%(EC/β^+) ^{213}Fr, see Fig. 4 of Ref. [10]. The α decay strongly populates the $3/2^-_1 \rightarrow 1/2^-_1 \rightarrow 5/2^-_{gs}$ sequence in ^{209}Rn where the $3/2^-$ state subsequently decays via a 104.8–110.3-keV cascade and a 214.9 keV crossover transition [2]. The $K_{\alpha 2}$ of francium and $K_{\alpha 1}$ of radon have similar energies, of 83.23 keV and 83.78 keV [24]. Thus, it is expected that the K_α lines to be coincident with the conversion electrons (CE) from both ^{213}Fr and ^{209}Rn nuclei. Therefore, the CEs with energies of 94, 106, and 116 keV observed in Fig. 11 of Ref. [12] might actually correspond to the CE_L (110 keV), CE_M (110 keV), and CE_K (215 keV) in ^{209}Rn. Since there is an order of magnitude difference between the evaluated conversion coefficients of the 104.8- and 110.3-keV transitions, α_k (104.8 keV; $M1$)/α_k (110.3 keV; $E2$) = 7.5(18)/0.362(5) [2], only the 110.3-keV transition is expected to contribute to the γ decay.

The highest four excited states in the range $E =$ 2.9–3.6 MeV can only be populated via the EC decay as $Q_{\beta^+} = 2.9$ MeV. The 3587- and 2877-keV states decay through rather high-energy transitions of 3088 keV and 2379 keV, respectively, directly to the $(7/2^-)_1$ state, see Figs. 1(b) and 2. The 3380-keV state decay path is made through the 2210–227–942-keV sequence of γ rays to the ground state. The 2950-keV state has several decay paths. Based on γ-γ coincidences, the most intense transitions form the 575–734–1143–498-keV and 400–909–1143–498-keV cascades.

Figure 1(c) shows that the 1300-keV transition feeding the 1170-keV state, is coincident with the 227–942-keV cascade and the 1128-keV γ ray. The γ-γ analysis and the energy balance for the 1170-keV state establishes that there exists a link between the 1170-keV and the 1128-keV states through the low-energy 42-keV γ ray. Therefore, the 42–1128-keV and the 227–942-keV cascades are parallel to each other. It should be noted that the energy of this transition has been deduced from the energy difference of the 1170- and 1128-keV excited states, while the intensity value quoted in Table I for the 42-keV transition has been deduced relative to the 227-keV transition and by considering that $I_{\gamma+IC}(42) \approx I_\gamma(1128)$ when observed in coincidence with the 1300-keV γ ray. The deduced total intensity $I_{\gamma+IC}(42)$ was 3.2(10)%, see Table I. Although no peak was observed above the background at 42 keV, an upper limit of $I_\gamma(42) < 0.4\%$ was estimated. Thus, the conversion coefficient has a lower limit of $\alpha(42) > 7$.

The existence of a 942-keV γ-ray doublet can easily be inferred by comparing Figs. 1(c)–1(e). The 521-keV and the 562-keV transitions are parallel, with similar intensities, see Table I, both depopulating the 1690-keV state. The 562-keV transition bypasses the 1170-keV state by feeding directly the 1128-keV level, and consequently, cannot be coincident with the 942-keV transition feeding the ground state. Therefore, the low 942-keV intensity seen in Fig. 1(e) is due to the contribution given by the higher-lying transition found to decay from the 2632-keV state. The spectrum presented in Fig. 1(d) shows the total 942-keV intensity since the 521-keV transition is coincident with both, while the spectrum in Fig. 1(c) includes only the contribution from the low-lying transition.

B. Log *ft* estimates

Considering that the conversion coefficients for the low-energy transitions in ^{213}Fr are expected to be significant, it is generally difficult to obtain the log ft values and the individual branching ratios for the β decay when there is poor knowledge of the spins, parities, transition multipolarities, and intensities. As the spin difference between the ground states of ^{213}Ra and ^{213}Fr is $4\hbar$, the ground state to ground state EC/β^+ decay is negligible.

The log ft values presented in Fig. 2 are calculated with the LOGFT CALCULATOR [29] considering the shape factor for the second forbidden nonunique transitions calculated as first-forbidden unique ($1u$), while the first-forbidden nonunique is calculated as an allowed β transition, as recommended by Turkat *et al.* [30]. The total γ+IC intensity to the ground state should equal the EC/β^+ decay branching ratio of 13(2) % and the absolute transitions intensities, presented in Fig. 2. The relative I_γ values presented in Table I are obtained by multiplying with the 0.066(10) factor.

The higher-lying states in the daughter nucleus are expected to be restricted to have rather low J values, due to the β decay selection rules and absence of γ feeding from higher-lying states, see the detailed discussion presented in Sec. V. The highest excited state, located at 3587 keV, has $I_{EC} =$ 0.22(5)% and log $ft = 5.32(11)$. The latter value corresponds to a presumably first-forbidden nonunique β transition if one compares it with the available experimental data [30] for $Z \geqslant 80$ heavier nuclei, see Fig. 3. Also, an allowed transition cannot be excluded. Thus, the ΔJ between the ^{213}Ra (g.s.) and the ^{213}Fr (3587-keV state) is expected to be of 0, $\pm 1\hbar$ units. The unique deexcitation path of the 3587-keV state through the 3088-keV γ ray directly to the $7/2^-_1$ state but not to the ground state, correlated with the $J^\pi = 1/2^-$ ground state of ^{213}Ra, indicates that it can be assigned a tentative value of $J^\pi = (1/2^+, 3/2^+)$. The half-lives of the states decaying via $E_\gamma > 3$ MeV, $M2$ or $E3$ [$(1/2^+, 3/2^+) \rightarrow 7/2^-_1$] transitions have single-particle values of the order of $T_{1/2} < 170$ ps.

The 2950-keV excited state decays mainly via low-energy transitions that have significant conversion coefficients, thus accurate EC intensities could not be calculated. However, using the γ-ray intensities, a $I_{EC} \approx 4.6(10)\%$ can be assigned to the EC feeding, resulting in a value of log $ft \approx 5.15(10)$. It

TABLE I. Properties of the excited states of ^{213}Fr: the excitation energy, E, the assigned spin and parity, J^π, the γ-ray energy for the decaying transitions, E_γ, the corresponding γ-ray intensity relative to the 498-keV transition considered to have $I_\gamma = 100$, I_γ, the γ-ray multipolarity assumption, the conversion coefficient, α_{tot}, and the total γ+IC intensity are listed. The α_{tot} was taken as the average of the minimum and maximum of the assumed multipolarity [25], with the uncertainty set to half their difference. Relative intensities were extracted from the γ-peak intensities in the singles spectrum. I_γ and $I_{\gamma+IC}$ intensities include the summing effect corrections. The spins and parities were assigned based on the comparison with the shell-model calculations (see Sec. IV), except where otherwise stated. The errors in E_γ are statistical. The energies of the excited states were obtained after a global minimization with GTOL software [26].

E [keV]	J^π	E_γ [keV]	I_γ[c] %	Multipolarity	α_{tot}	$I_{\gamma+IC}$ %
498.3(1)	$7/2^-$[d]	498.3(1)	100(6)	$M1(+E2)$	0.165(2)	116.5(70)
942.4(1)	$(7/2^-)$[e]	444.4(1)	1.0(1)	$(M1,E2)$	0.137(88)	1.1(1)
		942.4(1)	34.8(12)			34.8(12)
1128.1(1)	$(5/2^-)$[e]	1128.0(1)	35.2(12)			35.2(12)
1169.8(1)	$(3/2^-)$[e]	41.8(2)[a]	6.9(17)			6.9(17)
		227.4(1)	17.1(5)	$(E2)$	0.353(5)	23.1(7)
		671.4(1)	1.4(2)			1.4(2)
1641.0(1)	$(3/2^-)$[e]	1142.7(1)	105(6)			105(6)
1690.4(1)	$(1/2^-)$[e]	520.5(1)	7.0(3)	$(M1,E2)$	0.090(57)	7.6(5)
		562.2(1)	6.8(3)	$(E2)$	0.0281(4)	7.0(3)
1728.4(1)	$(5/2^-)$[e]	1230.0(1)	7.3(7)			7.3(7)
		1728.5(1)	3.1(2)			3.1(2)
1825.1(1)	$(5/2^-)$[e]	1326.7(1)	5.4(2)			5.4(2)
		1825.1(1)	7.6(5)			7.6(5)
1866.6(1)		738.6(1)	7.8(8)			7.8(8)
2374.9(1)		684.4(1)	1.8(2)			1.8(2)
		733.8(1)	38.0(16)			38.0(16)
		1205.1(1)	0.9(1)			0.9(1)
2469.5(1)		779.1(1)	3.1(1)			3.1(1)
		828.4(1)	6.0(2)			6.0(2)
		1299.7(1)	18.1(13)			18.1(13)
2549.8(1)		174.9(1)	1.2(2)	$(M1,E2)$	1.9(10)	3.5(14)
		724.8(1)	7.4(2)			7.4(2)
		821.4(1)	6.1(2)			6.1(2)
		908.7(1)	22.2(10)			22.2(10)
2611.1(1)		969.9(1)	4.0(2)			4.0(2)
		920.8(1)	0.6(1)			0.6(1)
2632.4(1)		257.4(1)	1.0(1)	$(E1,M1,E2)$	0.52(47)	1.5(5)
		765.8(1)	2.6(4)			2.6(4)
		942.2(2)	3.7(4)			3.7(4)
		1462.4(3)	2.4(2)			2.4(2)
2744.7(1)		1103.7(1)	2.2(2)			2.2(2)
		1574.9(1)	4.3(2)			4.3(2)
2800.0(1)		1109.4(1)	2.2(2)			2.2(2)
		1159.2(1)	1.3(1)			1.3(1)
2877.1(1)		2378.7(1)	2.0(2)			2.0(2)
2949.8(1)	$(1/2^+, 3/2^+)$[b]	317.3(1)	6.5(2)	$(M1,E2)$	0.34(22)	8.7(14)
		338.5(1)	4.2(4)	$(M1,E2)$	0.28(18)	5.4(9)
		400.0(1)	21.0(7)	$(M1,E2)$	0.18(12)	24.8(26)
		480.4(1)	4.2(1)	$(M1,E2)$	0.11(7)	4.7(3)
		574.9(1)	4.5(1)	$(E1,M1,E2)$	0.06(5)	4.8(3)
		1083.2(2)	0.8(2)			0.8(2)
		1308.8(1)	5.7(2)			5.7(2)
3027.4(1)		1386.3(1)	1.7(1)			1.7(1)
3380.1(2)		2210.3(1)	0.6(1)			0.6(1)
3586.7(1)	$(1/2^+, 3/2^+)$[b]	3088.3(1)	3.4(5)			3.4(5)

[a]For this transition, the intensity includes the total γ+IC value.
[b]Spins and parities assigned in this work based on the arguments presented in Sec. III B, see text for details.
[c]Multiply by 0.066(10) to obtain absolute intensities per 100 decays.
[d]The spins and parities of the g.s. and the first excited state are taken from Decman *et al.* [8] and confirmed by the present work.
[e]Determined by the SM calculations detailed in Sec. IV.

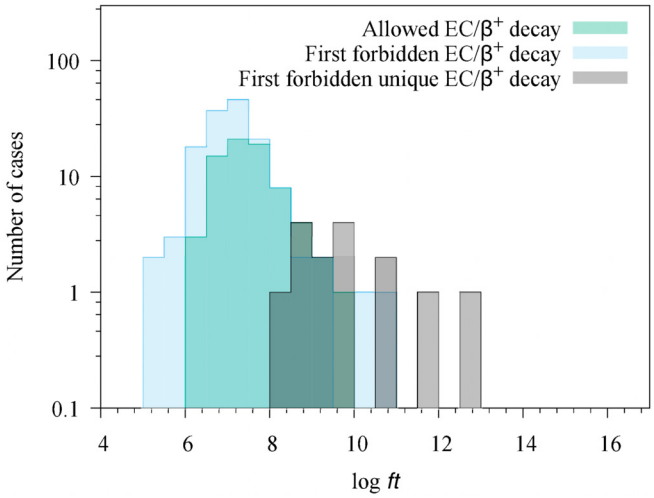

FIG. 3. Experimental log *ft* values for allowed and first-forbidden EC/β^+ decays for $Z \geqslant 80$. In the heavier mass region, the forbidden transitions compete with the allowed transitions making the forbidden transitions the dominant decay mode. The centroids of the log *ft* distributions for the first-forbidden EC/β^+ decays is 7.13(65) with slightly higher log $ft_C = 7.54(70)$ for allowed EC/β^+ decays. The numerical data are taken from the compiled data of Turkat *et al.* [30].

must be noted that the population of this state exhausts about 36% of the EC decay. The log *ft* value is most likely indicating a first-forbidden nonunique transition and therefore a tentative $J^\pi = (1/2^+, 3/2^+)$ value was assigned.

C. Half-life determination of the 1170-keV state

During the first run (see Sec. II for details), the 1170-keV state was found to be isomeric by measuring, with the HPGe detectors, the time distribution between the feeding 1300-keV and the deexciting 227-keV transitions. The half-life of the state was obtained through a two-step procedure, which included the energy correction of the time response and fitting the time distribution with an analytic function representing the convolution of the prompt time distribution with an exponential decay curve [31,32].

For this purpose, an $E_{\gamma,\mathrm{Start}}$–$E_{\gamma,\mathrm{Stop}}$–$\Delta T$ cube was built, where ΔT is the time stamp difference between any two HPGe crystals that detect a coincident pair of transitions, which populate and subsequently depopulate the state of interest. The time reference was chosen to be the average of the time stamps of the HPGe crystals in the event. The prompt distribution was constructed using a similar energy 1213–245 keV Start-Stop pair from the ^{152}Sm source to eliminate the energy dependence of the time response, see Fig. 4. The half-life of the 3^- state at 1579 keV from ^{152}Sm has an evaluated value of 72(6) fs [33] and it is negligible in comparison to the measured time resolution (FWHM) of the HPGe array of 43(1) ns for this pair of γ rays.

By fitting the 1170-keV state time distribution, presented in Fig. 4, with the convoluted function a half-life of 26(3) ns was obtained. Assuming an $E2$ character for the 227-keV transition (see Sec. IV), the strength becomes $B(E2)$=21(3) e^{2}fm^4 [0.271(36) W.u.]. For $A \approx 200$ nuclei and $E_\gamma \approx 200$ keV, the

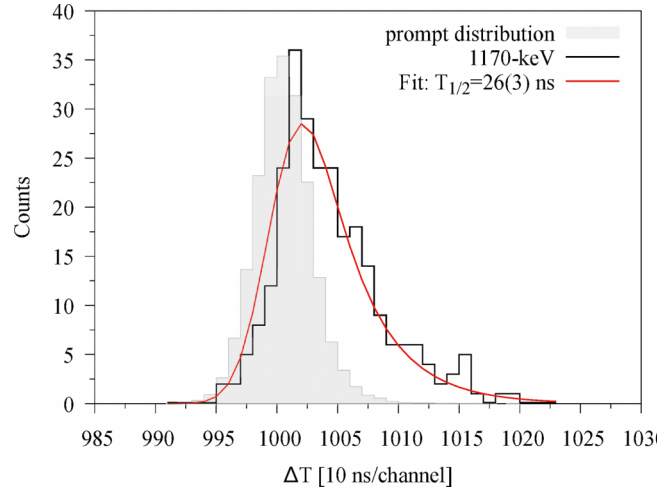

FIG. 4. The time distribution (as black line histogram) obtained for the 1170-keV state in ^{213}Fr using the 1300–227 keV Start-Stop pair of γ rays. From the fit of the distribution (red line), a half-life of $T_{1/2} = 26(3)$ ns was obtained. The prompt time distribution (grey shaded histogram) shows the $\tau = 0$ ns centroid used for the fit obtained using the 1213–245 keV from ^{152}Sm as Start-Stop selections. The error on the half-life value results from the fit. The reduced χ^2 test returned a value of 1.9.

experimental $B(E2)$ values between single- or multiparticle states generally fall below 1 W.u. [34].

D. Half-life determination of the 498-keV state

In the second run, the time distribution presented in Fig. 5 was obtained by considering the 1142–498-keV pair of

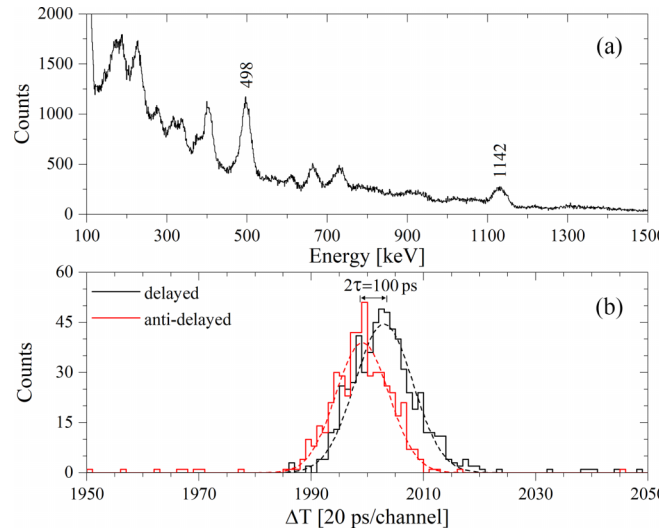

FIG. 5. (a) The total $LaBr_3$(Ce) energy projection from $E_{\gamma,\mathrm{Start}}$–$E_{\gamma,\mathrm{Stop}}$–$\Delta T$ cube. The labels represent the Start-Stop transitions, also shown in the energy HPGe spectrum of Fig. 1(a). Therefore, no contamination is expected to be included in the time distribution. (b) The double-gated time distribution obtained for the 498-keV state in ^{213}Fr. The centroid shift analysis gives a half-life upper limit of 35 ps.

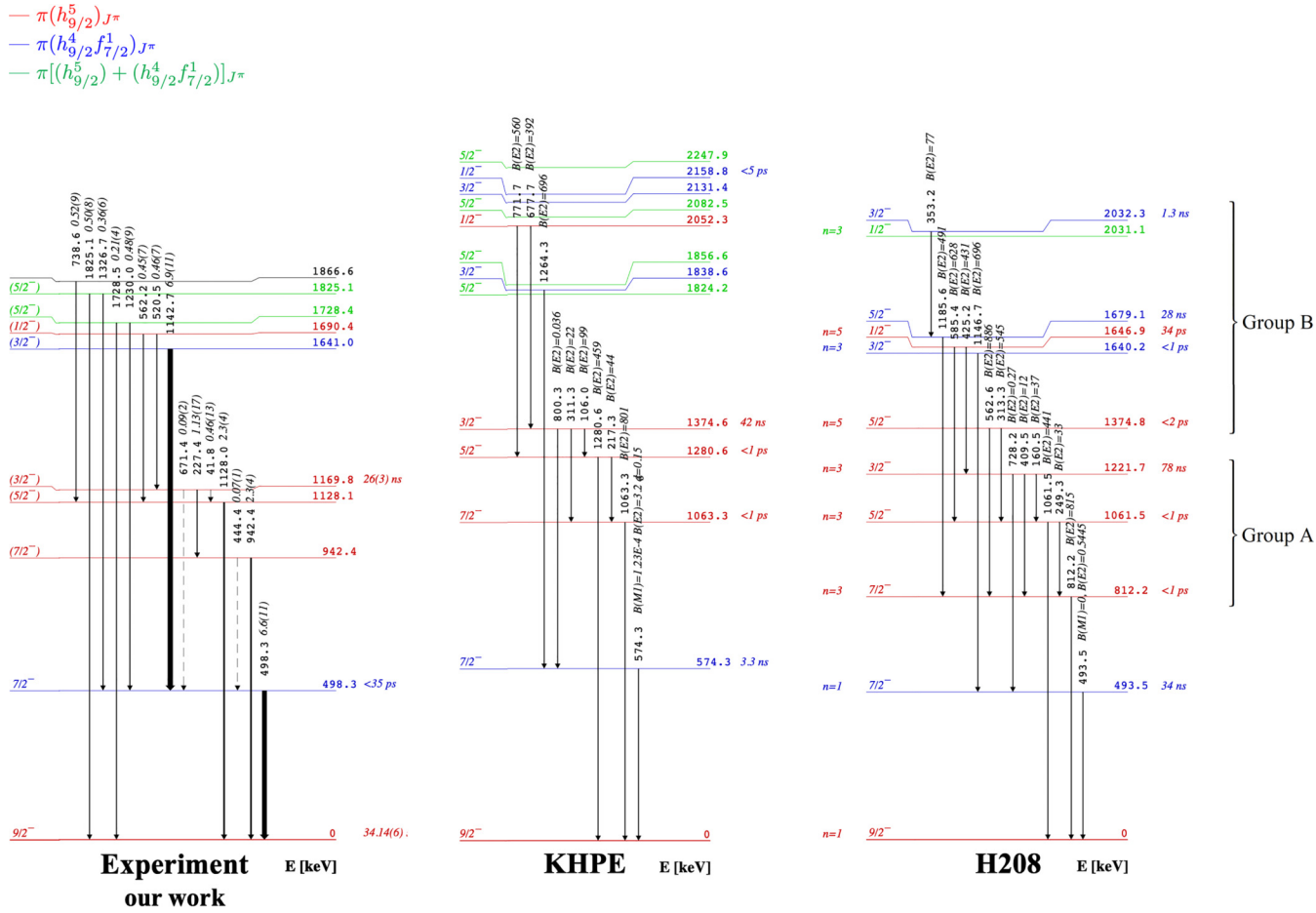

FIG. 6. The comparison between our partial experimental and the calculated ^{213}Fr level schemes with the KHPE [36] and *H*208 [39] interactions. The relevant part of the experimental level scheme includes the states up to about 2 MeV excitation energy. See Table II for the detailed wave-function compositions. The values above each decay represent the energy (in keV) and the calculated *E*2 and/or *M*1 transition probabilities (in units of e ^{2}fm^4 and/or μ_N^2). The seniority quantum number (ν), calculated with NATHAN [37], is indicated for each level. The colors indicate dominant configurations, as shown in the top-left corner.

coincident transitions by using the $LaBr_3$(Ce) subarray. The choice of the feeding-deexcitation γ rays was based on their experimentally determined intensity balance, see Table I and Fig. 1(a), combined with the selectivity of the $LaBr_3$(Ce) detectors presented in Fig. 5(a). From the centroid shift analysis an upper limit of $T_{1/2} \leqslant 35$ ps has been obtained. A pure $7/2^-_1 \rightarrow 9/2^-_{gs}$ *M*1 transition has the strength with a lower limit of the order of $9 \times 10^{-3}\mu_N^2$ ($\approx 5 \times 10^{-3}$ W.u.), while if a pure *E*2 multipolarity is assumed then $B(E2) = 526$ e ^{2}fm^4 ($\approx$7 W.u.). A detailed discussion regarding the possible *E*2 admixtures in this transition may be found in Secs. IV and V.

IV. SHELL-MODEL CALCULATIONS

Two independent shell-model (SM) calculations have been performed for ^{213}Fr (see Fig. 6): within the *jj*-coupling scheme with the NUSHELLX code [35] by using the KHPE diagonalization space [36] and with NATHAN [37,38] code, by using the *H*208 [39,40] interaction. Standard effective charges were used in the evaluation of the transition probabilities: $e_\nu = 0.5e$, $e_\pi = 1.5e$ for *E*2 transitions and $g^l_\pi = 1.$, $g^s_\pi = 5.586$, $g^l_\nu = 0$, and $g^s_\nu = -3.826$ for the spin and orbital factors for *M*1 transitions.

The configuration space for both interactions lies above the $Z = 82$ and $N = 126$ shell closures, and allows for the excitations of the 5 extra protons across the full $\pi\ 0h_{9/2}$ ($\epsilon_{spe} = -3799$ keV), $1f_{7/2}$ (-2902 keV), $0i_{13/2}$ (-2191 keV), $1f_{5/2}$ (-977 keV), $2p_{3/2}$ (-681 keV), $2p_{1/2}$ (-166 keV) single-particle orbits fixed in the Kuo-Herling effective interaction [36]. No neutron particle-hole excitations were considered above the Fermi level at $N = 126$ for the *H*208 and KHPE effective interactions, since ^{208}Pb is considered as closed core. No truncation was used in the calculations.

Although the experimental energy level scheme seems more compressed than the calculated ones, overall, a good agreement is found between the KHPE model predictions and the experiment, see Fig. 6, with $\Delta E = |E_{exp} - E_{th}| <$ 200 keV for the states from Group A. For Group B, ΔE remains around 200–400 keV. The KHPE theoretical level scheme closely follows the group structure exhibited by the experimental one. The energy gap between the states belonging to Group A and Group B is $\Delta(\text{GroupB} - \text{GroupA})_{EXP} \approx$ 470 keV for the experimental level scheme. This gap is

TABLE II. Major proton configurations $|J_\nu = 0^+, J_\pi, J\rangle$ basis states up to about 2 MeV excitation energy with the KHPE [36] and $H208$ [39] effective interactions. J and π represent the spin and parity of the state, N designates the index of state with the same J, and the predicted energy positions, E, from this work and previous calculations of Teruya *et al.* [42]. The positive parity low-J states are expected to only appear above 2.6 MeV, as it results from Sec. V. Only the components with amplitudes exceeding 3% are listed.

KHPE									
J	π	N	E [MeV]	E [a] [MeV]	$h^5_{9/2}$	$h^4_{9/2}f^1_{7/2}$	$h^3_{9/2}f^2_{7/2}$	$h^2_{9/2}f^3_{7/2}$	$h^3_{9/2}i^2_{13/2}$	$h^2_{9/2}f^1_{7/2}i^2_{13/2}$
			This work	Teruya *et al.* [42]						
9/2	-	1	0.000	0.000	0.38		0.22		0.24	
7/2	-	1	0.574	0.560		0.48		0.16		0.24
7/2	-	2	1.063	0.914	0.55		0.19		0.18	
5/2	-	1	1.281	1.030	0.53		0.20		0.19	
3/2	-	1	1.375	1.112	0.62		0.16		0.17	
9/2[b]	-	2	1.452	1.219	0.59		0.18		0.18	
7/2[b]	-	3	1.772	1.713		0.64		0.12		0.16
5/2	-	2	1.824	1.301	0.70	0.12			0.03	0.03
3/2	-	2	1.839	1.713		0.64		0.10		0.15
5/2	-	3	1.856	-	0.17	0.48		0.11		0.13
1/2	-	1	2.052	1.507	0.89		0.03		0.03	
3/2	-	3	2.131	-		0.69		0.11		0.15
1/2	-	2	2.159	1.993		0.65		0.09		0.14
$H208$										
J	π	N	E [MeV]		$h^5_{9/2}$	$h^4_{9/2}f^1_{7/2}$	$h^3_{9/2}f^2_{7/2}$	$h^2_{9/2}f^3_{7/2}$	$h^3_{9/2}i^2_{13/2}$	$h^2_{9/2}f^1_{7/2}i^2_{13/2}$
			This work							
9/2	-	1	0.000		0.52		0.16		0.22	
7/2	-	1	0.494			0.59		0.10		0.22
7/2	-	2	0.812		0.68		0.12		0.14	
5/2	-	1	1.062		0.68		0.12		0.14	
3/2	-	1	1.222		0.72		0.10		0.13	
9/2[b]	-	2	1.334		0.72		0.11		0.13	
5/2	-	2	1.375		0.88	0.03			0.04	0.03
7/2[b]	-	3	1.608			0.71		0.09		0.14
3/2	-	2	1.640			0.71		0.06		0.13
1/2	-	1	1.647		0.90				0.04	
5/2	-	3	1.679			0.69	0.10			0.13
1/2	-	2	2.031			0.72	0.04	0.05		0.11
3/2	-	3	2.032			0.76		0.07		0.12

[a]The level energies of Teruya *et al.* [42] were obtained in a large-scale shell-model calculations including all six π $0h_{9/2}$, $1f_{7/2}$, $0i_{13/2}$, $1f_{5/2}$, $2p_{3/2}$ and $2p_{1/2}$ orbitals between N=82 and 126. The numerical data was digitized from their Fig. 11 using DigitizeIt https://www.digitizeit.xyz.
[b]The $7/2^-_3$ and $9/2^-_2$ states were calculated only for completeness, since both states are expected to be hindered by the EC/β^+ decay selection rules.

well reproduced by the KHPE interaction, $\Delta(\text{GroupB} - \text{GroupA})_{\text{KHPE}} \approx 449$ keV.

With the $H208$ interaction, an agreement of the order of $\Delta E = |E_{\text{exp}} - E_{\text{th}}| < 100$ keV is found for most of the states in the two groups, A and B. However, the position of the $5/2^-$ states at 1375 keV, with other ones of spins ($7/2^-$, $9/2^-$), reported in Table II, leads to a disappearance of the gap structure between the two groups.

The calculated $B(E2)$ values presented in Fig. 6 emphasize that there are enhanced $E2$ transition probabilities of the order of hundreds of $e^2\text{fm}^4$ between states with a seniority change of $\Delta\nu = \pm 2$ units ($\nu = 5 \rightarrow \nu = 3$ or $\nu = 3 \rightarrow \nu = 1$, respectively) while between the states with $\nu = 3$ are mostly weak, of a few tens of $e^2\text{fm}^4$ at most. As emphasized by Ressler *et al.* in their Figs. 1(a) and 2(a) [41], a minimum in $B(E2)$ is reached for transitions that conserve the seniority, $\Delta\nu = 0$, for nuclei nearby closed shells and for a fractional filling of the j shell of $f = n/(2j+1) = 0.5$, where, in this case, the $E2$ transition is of the order of $(1-2f)^2$. On the contrary, the opposite situation is encountered for the $\Delta\nu = \pm 2$ transitions where the $B(E2)$ is maximized for half-filled orbits.

For $j = (9/2)^5$ configurations, the lowest seniority-one state has $J = 9/2^-$. Up to three states with $J = 1/2^-$, $3/2^-$, $5/2^-$, $7/2^-$, and $9/2^-$ in ^{213}Fr were calculated at low and medium excitation energy. Their SM configurations are detailed in Table II. Since states with spins $J > 7/2$ are not expected to be directly populated at a measurable rate in the

^{213}Ra($1/2^-$) EC/β^+ decay (as shown also in Fig. 2), only one excited $9/2^-_1$ state has been calculated since it is expected to be part of the group of states with seniority $\nu = 3$.

The spin and parity of the ground state $J^\pi = 9/2^-$ and the first excited state $J^\pi = 7/2^-$ are supported by both shell-model calculations. The $J^\pi = 7/2^-$ value is adopted for the first excited state, thus confirming the value of Mayer *et al.* [8]. The configurations at excitation energies below 3–4 MeV are dominated by the strongly bound orbits $\pi 0h_{9/2}$, $1f_{7/2}$ and, at most, $0i_{13/2}$, with an energy gap of about $|\epsilon(\pi h_9, 1f_7, 0i_{13}) - \epsilon(\pi 1f_5, 2p_3, 2p_1)| \approx 2$–$3$ MeV.

Our calculations are compared with the energy levels and $B(E2)$ values determined using a large-scale SM approach performed by Teruya *et al.* [42] using the same diagonalization space and proton single-particle energies, $\varepsilon_{\rm spe}$. The list of excitation energies obtained for ^{213}Fr by Teruya *et al.* is presented in Table II. The theoretical $B(E2)$ values were obtained using the renormalized effective charges $e_\nu = -0.85e$, $e_\pi = 1.5e$ [42].

A. $J^\pi = 7/2^-_1$ one-quasiparticle state

The energy position calculated with KHPE[$H208$] (notation used hereafter) is 574[494] keV, which is consistent with the experimental value, see Table I, and the value obtained by Teruya *et al.* of 560 keV [42], see Table II. Our SM calculations predict a structure dominated by the 48%[59%]$(h^4_{9/2}f^1_{7/2})$ + 40%[32%][$(h^2_{9/2}f^3_{7/2})$ + $(h^2_{9/2}f^1_{7/2}i^2_{13/2})$] proton configurations, see Table II.

For the $7/2^-_1 \rightarrow 9/2^-$ transition, the KHPE SM predicts a $B(E2) = 3.2$ e^{2}fm^4 and a severely hindered $B(M1) = 1.23 \times 10^{-4}\ \mu_N^2$ component. It results in a calculated half-life of $T_{1/2}(\gamma) = \ln(2)/[\lambda(M1) + \lambda(E2)] = 3.3$ ns, where $\lambda(M1)$ and $\lambda(E2)$ represent the theoretical transition rates. The theoretical value deviates from the experimental value by two orders of magnitude. This result agrees with the conclusion of the survey of Govil and Khurana [43] performed over a set of experimental lifetimes of l-forbidden $M1$ transitions for $N = 28$–126 nuclei, where the experimental matrix elements showed minima at magic neutron numbers. The $H208$ interaction predicts a $B(E2) = 0.55$ e^{2}fm^4, which gives $T_{1/2} = 34$ ns.

Teruya *et al.* [42] calculated a pure $E2$ transition in ^{213}Fr with a strength of 1.056 W.u., which predicts a lifetime of about 240 ps. This result is about a factor 10 higher than what was found experimentally in this work. A core excitation calculation for ^{209}Bi of Kratschmer *et al.* [44] showed a fair agreement with the experimental value of the half-life of the $7/2^-$ state. They found that the expected hindrance factor for the $M1$ transition is of the order of 10^{-3} W.u. while the strength of the $E2$ part is of the order of 2 W.u. Additionally, their shell-model calculation also underestimates the $B(E2)$ by a factor of 15. Therefore, the SM obviously fails to reproduce the experimental value.

B. Group A: $\pi(h^5_{9/2})_{J^\pi}$ ground-state multiplet of states

The assignment of the 942-, 1128-, 1170-, 1690-keV states with a J^π of $7/2^-_2$, $5/2^-_1$, $3/2^-_1$ and $1/2^-_1$ was made based on the comparison with the SM, as shown in Fig. 6. Table II contains the predictions given by our KHPE[$H208$] SM calculations compared with Teruya *et al.* [42]. Both SM calculations seem to give, consistently, higher-energy positions for the $\pi(h^5_{9/2})_{J^-}$ states in the case of the KHPE and $H208$ interactions by about 200 and 100 keV, respectively. The energy spectrum of Teruya *et al.* [42] seems more compressed.

Their intrinsic structure together with the $9/2^-_{\rm gs}$ state is dominated by the $\pi(h^5_{9/2})_{J^\pi}$ configuration, which accounts for around 40–90 % of the their total wave function amplitude, the rest being shared between the $\pi(h^3_{9/2}f^2_{7/2}) + (h^3_{9/2}i^2_{13/2})$ configurations, see Table II for details. These two terms show that their structure is dominated by the pair of protons coupled to 0^+ scattered from $h^{-2}_{9/2}$ to either $f^2_{7/2}$ or $i^2_{13/2}$ higher orbits. The states of a multiplet are expected to be solely linked by $E2$ transitions, unless configuration mixing occurs. Similar situations are encountered in nuclei close to magic ($Z = 20$, $N = 20$), ($Z = 82$, $N = 126$) numbers [45–48].

The $1/2^-_1$ state has a ≈90% $\pi(h^5_{9/2})$ configuration. This state seems to closely resemble a pure state while the other low-lying members deviate significantly from this value, see the results summarized in Table II. This conclusion is in accordance with the expectation that the ground state has a more mixed character since the pairing interaction mixes the higher-lying $J = 0$ pairs of nucleons. $J^\pi = 1/2^-$ assignment for the 1690-keV state is based on its decay pattern through the 521-kev and 562-keV γ rays to the $3/2^-_1$ and $5/2^-_1$ states, which implies a similarity in the structure of the states. Strong $E2$ transition strengths of $B(E2; \rightarrow 3/2^-_1) = 392[431]$ e^{2}fm^4 and $B(E2; \rightarrow 5/2^-_1) = 560[628]$ e^{2}fm^4, respectively are predicted by the KHPE[$H208$] interactions for the parallel pair of transitions. Both interactions give consistent $E2$ transition strengths which validate the $J^\pi = 1/2^-$ assignment for the 1690-keV state.

The SM calculations performed for the $3/2^-_1$ isomeric state at 1170 keV, decaying to the $5/2^-_1$, $7/2^-_2$, and $7/2^-_1$ states through the 42-, 227-, and 671-keV transitions (see Fig. 6) indicates that the transitions are mainly of $E2$ character, with a strongly hindered $M1$ component with the strength of the order of $B(M1) \approx 10^{-5}\mu_N^2(\rightarrow 5/2^-)$, see Tables III and IV for details. The KHPE[$H208$] calculated transition strengths $B(E2)$ to the $5/2^-_1$, $7/2^-_1$ and $7/2^-_2$ states are equal to 99[37], 22[12], and 0.036[0.27] e^{2}fm^4, respectively. These values are in good agreement with the experimentally determined values of 65.1 (148), 19.3(25), and 7.11(134) $\times 10^{-3}$ e^{2}fm^4. The calculated level half-life of 42[78] ns is significantly overestimated when compared with the experimental value.

The $5/2^-_1$ state uniquely deexcites through the intense 1128-keV transition to the ground state. The theoretical $B(E2)$ is predicted to give a strength of 459[441] e^{2}fm^4, which yields a half-life in the subpicosecond range. Also, a weak $E2$ transition is predicted to the $7/2^-_2$ state with a $B(E2)$ strength of 44[33] e^{2}fm^4. This transition has not been observed experimentally.

The $3/2^-_1$ and the $7/2^-_2$ states were the only members within Group A experimentally found to decay to the $7/2^-_1$ state via the 671- and 444-keV weak transitions

TABLE III. Partial half-lives estimates for the 42-, 227- and 671-keV transitions depopulating the $(3/2^-)$ isomer at 1170 keV. A pure E/M $\Delta L = 1$, 2 character is assumed for each transition. The partial half-lives are obtained (see Sec. III C) from the measured half-life as: $T_{1/2}(\gamma_k) = T_{1/2}(\text{level}) \sum_{i=1}^{n} (I_{\gamma i}) \frac{(1+\alpha_i)}{I_{\gamma k}}$ [49] by using the γ-rays energies and experimentally determined branching ratios, see Table I. The values corresponding to the 42-keV transition are calculated assuming an $E2$ conversion coefficient for the 227-keV transition. The ICCs, $\alpha_{\text{tot}}^{\text{th}}$, are those calculated with BRICC [25]. $T_{1/2}^{\text{th}}$ is the Weisskopf estimate for each multipolarity and B is defined as $T_{1/2}^{\text{th}}/T_{1/2}^{\text{part}}$.

E_γ (keV)	Multipolarity	$\alpha_{\text{tot}}^{\text{th}}$	$T_{1/2}^{\text{part}}$(ns)	$T_{1/2}^{\text{th}}$(ns)	B(W.u.)	B$\left(\mu_N^2 \text{ or e}^2\text{fm}^4\right)$
41.8(2)	$M1$	36.1(8)	$4.39(99) \times 10^3$	0.301	$6.86(155) \times 10^{-5}$	$1.23(28) \times 10^{-4}$
	$E2$	577(16)	$6.81(155) \times 10^4$	5.87×10^4	0.86(20)	65.1(148)
227.4(1)	$M1$	1.408(20)	75.2(91)	1.87×10^{-3}	$2.49(30) \times 10^{-5}$	$4.46(54) \times 10^{-5}$
	$E2$	0.353(5)	47.8(61)	12.2	0.256(33)	19.3(25)
671.4(1)	$M1$	-	583(110)	7.27×10^{-5}	$1.24(23) \times 10^{-7}$	$2.23(42) \times 10^{-7}$
	$E2$	-	583(110)	5.49×10^{-2}	$9.41(177) \times 10^{-5}$	$7.11(134) \times 10^{-3}$

$(I_\gamma < 0.1)$, see Fig. 2. Theoretical $B(M1) \approx 10^{-3}$ μ_N^2 and $B(E2) \approx 10^{-3}$–10^{-4} e^{2}fm^4 estimates were obtained for the $J \to 7/2_1^-$ decays, thus confirming the experimental observations.

C. Group B: Mixed structure states

$3/2_2^-$ *1641-keV state.* This state uniquely decays through the 1143-keV transition. The high experimental intensity found for this γ ray to the $7/2_1^-$ state is an indication of the significant overlap in their wave functions. Possible candidates with dominant one quasiparticle character, $\pi(h_{9/2}^4 f_{7/2}^1)$, are the $3/2_2^-$, $5/2_4^-$, $3/2_3^-$, and $1/2_2^-$, see Table II. The reasonable spin assumption is $J^\pi = 3/2_2^-$ for this state, since all the others are predicted to appear at $\geqslant 2$ MeV excitation energy. A second argument is given by the significant EC feeding, see Fig. 2. The KHPE[H208] calculated $B(E2)$ values of 669[696] e^{2}fm^4 is in line with a $\Delta\nu = 2$ change γ-ray transition, see Fig. 6 for details.

$5/2_2^-$ *1728- and* $5/2_3^-$ *1825-keV states.* Both states have identical decay patterns with pairs of parallel transitions (1230 keV; 1728 keV) and (1327 keV; 1825 keV) to the $7/2_1^-$ and $9/2_{\text{gs}}^-$ states, respectively. The most suitable assignment is $J^\pi = 5/2^-$ since both $5/2_{2,3}^-$ states are predicted by the KHPE interaction to have a mixed configuration between the main components of the $7/2_1^-$ and the $9/2_{\text{gs}}^-$ states. As detailed in Table II, the structure of the $5/2_2^-$ state in the $H208$ calculation accounts for about 88% contribution from the $\pi(h_{9/2}^5)_{5/2}$ configuration which favors a lowering in the energy. While the KHPE interaction predicts a more mixed character for the $5/2_{2,3}^-$ states, the $H208$ interaction gives rather pure wave functions.

V. DISCUSSION

A. Decay scheme of ^{213}Fr

The weak 444- and 671-keV transitions with hindrance factors of $I_\gamma(942)/I_\gamma(444) \approx 40$ and $I_\gamma(227+42)/I_\gamma(671) \approx 20$ were found to link the $7/2_2^-$ and $3/2_1^-$ states with the one-quasiparticle $7/2_1^-$ state thus pointing towards configuration mixing. Indeed, the states within Group A show a preference to decay directly to the $9/2_{\text{gs}}^-$ rather than to the $7/2_1^-$ state. As shown in Fig. 7, the Group A–$7/2_1^-$–$9/2_{\text{gs}}^-$ sequence of states and their subsequent γ decays resemble the ^{211}At nucleus [3]. The main difference is that the intense $3/2_1^- \to 7/2_1^-$ decay in ^{211}At indicates a strong configuration mixing which might be favored by the more compressed spectrum, see Fig. 7.

1. Group A: $\nu = 3$ proton multiplet

1170-keV state. From the SM calculations, a tentative $(M1)+E2$ character can be assigned to the 42-keV γ ray,

TABLE IV. The $E2$ transition probabilities for the $3/2_1^-$ isomer decay in ^{213}Fr and ^{211}At. For the experimentally obtained $B(E2)$ values in ^{213}Fr see Table. III.

	^{213}Fr			^{211}At		
	(This work)			Ref. [4]		
Transition	$E_{\gamma,\text{exp.}}$	B(E2)$_{\text{KHPE}}$	B(E2)$_{\text{H208}}$	$E_{\gamma,\text{exp.}}$	$B(E2)_{\text{Exp.}}$	$B(E2)_{\text{Th.}}$[a]
$3/2_1^- \to$	(keV)	(e^{2}fm^4)	(e^{2}fm^4)	(keV)	(e^{2}fm^4)	(e^{2}fm^4)
$\to 5/2_1^-$	41.8	99[b]	37	168.7	955(105)[c]	220
$\to 7/2_2^-$	227.4	22	12	250.2	135(14)	32
$\to 7/2_1^-$	671.4	3.6×10^{-2}	0.27	442.2	34(2)	-

[a]The proton effective charges used in the calculations are: $e_\pi = 2.04 \pm 0.10$e for the $(h_{9/2}^3)_{3/2_1^-} \to (h_{9/2}^3)_{5/2_1^-}$ transition and $e_\pi = 2.06 \pm 0.10$e for the $(h_{9/2}^3)_{3/2_1^-} \to (h_{9/2}^3)_{7/2_2^-}$ transition. See Table 1 of Ref. [50] and Ref. [4] for details.

[b]The KHPE interaction also predicts for the $3/2_1^-$ and $5/2_1^-$ transition an $M1$ strength of B(M1) $= 0.7 \times 10^{-4} \mu_N^2$.

[c]The experimentally determined $M1$ strength in the ^{211}Rn EC decay is $B(M1) = 2.3 \times 10^{-4}$ μ_N^2 [4].

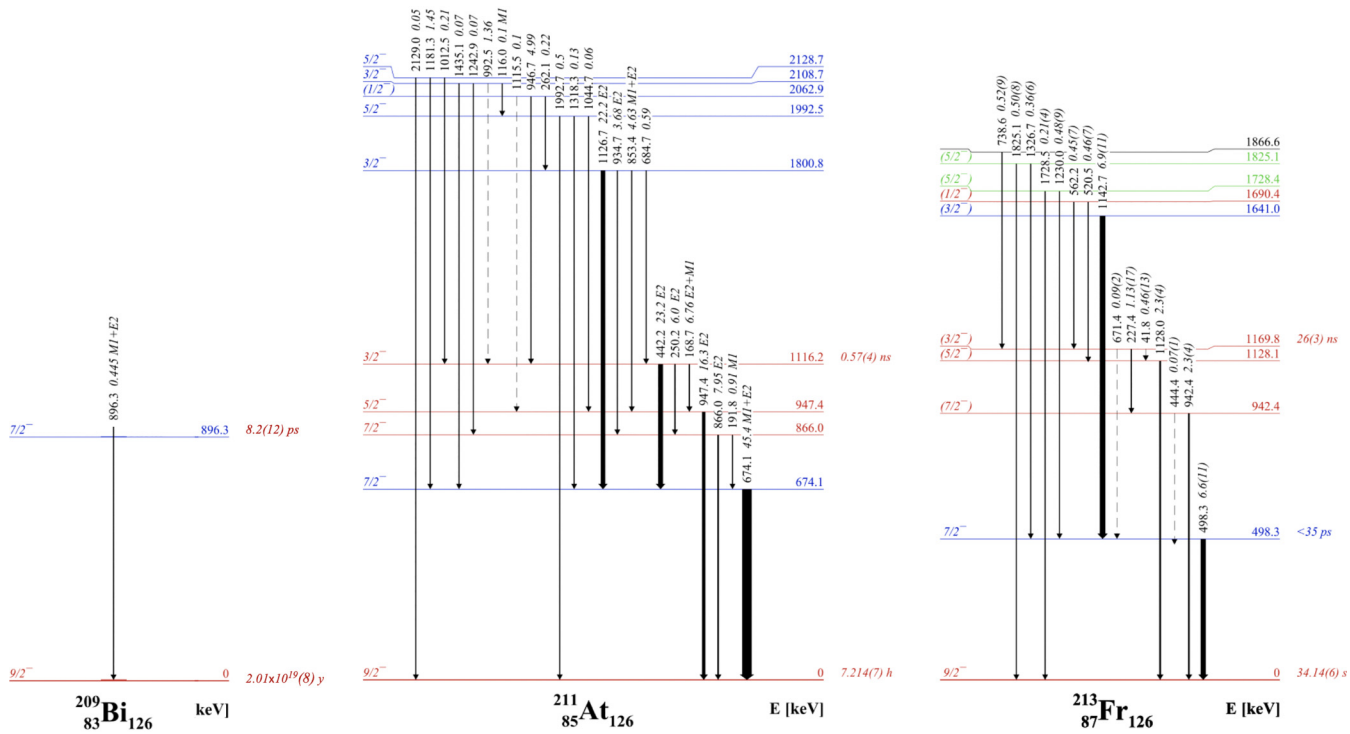

FIG. 7. The experimental EC/β^+ decay schemes of the $N = 126$ isotones: ^{209}Bi [2], ^{211}At [3–5,15], and ^{213}Fr (this work). Only the states up to ≈2 MeV excitation energy are included. All the γ-ray intensities are absolute values. The same color code indicating dominant configurations applies as in Fig. 6.

while the 227- and 671-keV transitions can be regarded as pure $E2$. Since the $3/2^-_1$ (isomeric) and the $5/2^-_1$ states originate from the $\pi(h^5_{9/2})_{J^\pi}$ multiplet, the $M1$ component is forbidden and signals configuration mixing in this case. Likewise, the observation of the weak 671-keV, $3/2^- \rightarrow 7/2^-_1$, transition hints towards some admixture in the initial state resembling the $\pi[\alpha(h^5_{9/2}) + \beta(h^4_{9/2}f^1_{7/2})]_{J^\pi}$ configuration or the $\alpha[^{212}\mathrm{Rn}(0^+) \oplus \pi(f^1_{7/2})] + \beta[\pi(h^5_{9/2})]$ configuration in the final state. An $E2$ $\pi(h^5_{9/2})_{J^\pi} \rightarrow \pi(h^4_{9/2}f^1_{7/2})_{J^\pi}$ transition between pure states is forbidden in this approximation.

2. States above 2 MeV

The intrinsic structure of the ground state of ^{213}Ra parent nucleus is dominated by the $\nu p^{-1}_{1/2} \otimes \pi[^{214}\mathrm{Ra}(0^+_1)]$ configuration with a minor contribution stemming from $\nu f^{-1}_{5/2} \otimes \pi[^{214}\mathrm{Ra}(2^+_1)]$, as shown by Gerathy *et al.* [51]. As pointed by Hansen [52], in the region of the double closed shell ($Z = 82$, $N = 126$), the only allowed transition can proceed via $\pi 2f_{7/2} \rightarrow \nu 2f_{5/2}$. All other decays are of first-forbidden character since the accessible valence orbits, for protons and neutrons, are of alternating parity and relatively high angular momentum (π $h_{9/2}$, $f_{7/2}$, $i_{13/2}$ and ν $g_{9/2}$, $i_{11/2}$, $j_{15/2}$) while the orbitals near the Fermi surface are low-l, π $s_{1/2}$, $d_{3/2}$, and ν $p_{1/2}$, $f_{5/2}$, $p_{3/2}$, respectively. Caurier *et al.* [53] showed that in the case of the $N = 126$ isotones, the occupation number for the $f_{7/2}$ orbit is monotonically increasing with proton number, reaching the value of 1 for $Z = 88$ (Ra). This fact directly affects the amplitude of the allowed EC/β^+ decay. Conversely, in the medium mass region, shell-model equivalent orbits are encountered for protons and neutrons and, therefore, the allowed β decays dominate. Therefore, in the ^{213}Ra $\rightarrow$ ^{213}Fr EC decay, there are several possible scenarios [(i)–(iv)] given the fact that simply converting a $\pi h_{9/2} \rightarrow \nu p_{1/2}$ requires a high angular momentum change.

(i) A core $s_{1/2}$ or a $d_{3/2}$ proton is involved and captures a K-shell electron subsequently converting into a $p_{1/2}$ neutron thus completely filling the $N = 126$ major shell. As summarized by Hansen [52] and also pointed by Astner [3], the first-forbidden EC ($\Delta l = 1$) $\pi s_{1/2}$ or $\pi d_{3/2}$ $\rightarrow \nu p_{1/2}$ transition was experimentally observed to be favored in the $Z \geqslant 82$, $A \approx 200$ region. For ^{213}Fr it leads to positive parity, low $J \leqslant 1/2$ or $3/2$ states directly populated at high excitation energies. This expectation is supported by the experimentally determined log ft values for the 3587- and the 2950-keV states. All positive $1/2^+$ and $3/2^+$ states are predicted by the SM calculation to appear at energies exceeding 2.7 MeV.

(ii) A $f_{7/2}$ proton is converted into a $f_{5/2}$ neutron. Given the small $\nu f^{-1}_{5/2} \otimes \pi[^{214}\mathrm{Ra}(2^+_1)]$ contribution in the parent ground state wave function, it is expected that these allowed β transitions populate with a low feeding negative parity states in the ^{213}Fr daughter nucleus.

(iii) Another EC decay path to fill the $f_{5/2}$ neutron hole is to convert the bound $d_{3/2}$ proton by a first-forbidden transition.

(iv) The unhindered first-forbidden $\pi h_{9/2} \rightarrow \nu g_{9/2}$ decay may be energetically favorable to populate neutron

$\nu(g_{9/2}\, p_{1/2}^{-1})$ states located at relatively high excitation energy. This result has been reported by Jardine [48] for the ^{210}At → ^{210}Po EC decay at energies nearby the Q value.

B. 498 keV: A possible *l*-forbidden M1 transition

The intense 498-keV decay of the $7/2^-$ state can be regarded as having a dominant l-forbidden magnetic dipole character (see Sec. I and references therein). In a nonrelativistic approach the $\pi f_{7/2} \rightarrow \pi h_{9/2}$ transition is strictly forbidden between orbits with $\Delta l \neq 0$. Assuming a $M1{+}E2$ character with a mixing ratio of about 0.62–0.65 [2,5,14] found in the ^{209}Bi and ^{211}At $N = 126$ isotones for their similar transitions then the partial strength for the $M1$ part is of the order of $9 \times 10^{-3}\mu_N^2$ ($\approx 5 \times 10^{-3}$ W.u.) while for the $E2$ component is about 227 e^{2}fm^4 ($\approx$3 W.u.).

C. ^{209}Bi – ^{211}At – ^{213}Fr $N = 126$ chain

In the odd-A $^{209}\mathrm{Bi}_{126}$–$^{211}\mathrm{At}_{126}$–$^{213}\mathrm{Fr}_{126}$–$^{215}\mathrm{Ac}_{126}$ chain of isotones all ground states have $J^\pi = 9/2^-$ [2,5,27] and first-excited states have $J^\pi = 7/2^-$, see Fig. 7. A lowering of the one-quasiparticle $7/2_1^-$ state is observed as pairs of protons are added to the ^{208}Pb core. It was shown by Caurier *et al.* [53] that due to pairing, in the $N = 126$ isotones, the $\pi(h_{9/2}^n)_{9/2^-}$ configuration amounts about 60% in $_{84}$Po and $_{85}$At and further decreases to 40% in $_{86}$Rn and $_{87}$Fr, to 20% in $_{88}$Ra and $_{89}$Ac and to nearly 0% in $_{91}$Pa and $_{92}$U in the ground state wave function structure.

The medium and low-energy structure of ^{211}At studied in the ^{211}Rn EC decay shows a multiplet of states based on the $\pi(h_{9/2}^3)_{J^-}$ configuration linked through $E2$ transitions or directly decaying to the ground state [45]. Figure 7 shows a few important similarities between the $N = 126$ isotones below 2 MeV excitation energy. A common feature of the $7/2_1^- \rightarrow 9/2_{gs}^-$ decay in ^{209}Bi and ^{211}At is the mixing ratio of $\delta = -0.62(6)$ [2,14] and $-0.65(6)$ [5], that remains rather constant for both nuclei. The main components in the structure of the two states are expected to be $(h_{9/2}^{n-1} f_{7/2})$ and $(h_{9/2}^n)$ in ^{209}Bi, ^{211}At and ^{213}Fr. Therefore, all three nuclei seem to exhibit l-forbidden $M1$ character transitions at low excitation energy.

The $3/2_1^-$ state is isomeric in both ^{211}At and ^{213}Fr nuclei and decays via γ-rays transitions to the $5/2_1^-$, $7/2_2^-$, and $7/2_1^-$ states. A direct comparison of intensities for the 442-keV transition (^{211}At) and the similar 671-keV decay (^{213}Fr), as presented in Fig. 7, hints towards the conclusion of a higher purity of the isomeric $3/2^-$ state in ^{213}Fr in terms of $(h_{9/2}^n)_{3/2}$ configuration. The 250- and the 227-keV $3/2_1^- \rightarrow 7/2_2^-$ and the 168- and the 42-keV $3/2_1^- \rightarrow 5/2_1^-$ transitions are predicted to be of $\nu = 3 \rightarrow 3$ pure $E2$ character, see Tables III and IV for details.

A deviation from the expectation of low strength $E2$ γ decays between states with no change in seniority quantum number ($\Delta\nu = 0$) is found in ^{211}At. The experimentally determined $E2$ transition rate between the $3/2_1^-$ and $5/2_1^-$ members of the j^3 multiplet was found to be 995(105) e^{2}fm^4, which is about ten times higher in ^{211}At than in ^{213}Fr, see Table IV. This value is in contradiction with their theoretical value $B(E2, 3/2_1^- \rightarrow 5/2_1^-) = 220$ e^{2}fm^4. Astner *et al.* [50] acknowledged the inconsistency between the rather high $B(E2)$ value between states with the same seniority ($\nu = 3$).

VI. SUMMARY AND CONCLUSIONS

A detailed level scheme of ^{213}Fr was built up to an excitation energy of 3.6 MeV following the EC decay of ^{213}Ra ($1/2_{g.s.}^-$). The spin and parity were confirmed for the first $7/2^-$ excited state at 498 keV. A tentative spin and parity assignment is made for the majority of the newly found states based on the systematics of the $N = 126$ isotones and two independent shell-model calculations performed with the KHPE and $H208$ effective interactions. An upper limit of 35 ps is determined for the half-life of the $7/2_1^-$ state. The $7/2_1^- \rightarrow 9/2_{g.s.}^-$ decay is a suitable candidate for an l-forbidden $M1$ character transition. This assumption is based on the similarities with the adjacent ^{209}Bi and ^{211}At nuclei and it is also supported by the shell-model calculations.

The experimental decay scheme seems to be organized in groups (Group A and Group B). Group A comprises the seniority $\nu = 3$ $7/2_2^-$, $5/2_1^-$, $3/2_1^-$, and $1/2_1^-$ states with a dominant $\pi(h_{9/2}^5)$ configuration, while Group B contains higher-lying, more mixed states having seniority $\nu = 3$ and 5.

A nanosecond isomeric state, with a half-life of 26 ns and a tentative $J^\pi = (3/2^-)$ has been identified at rather low excitation energy of 1170 keV. The rather small $E2$ strengths for the $3/2_1^-$ → Group A transitions of a few tens of e^{2}fm^4 follows the parabolic behavior exhibited by the $B(E2)$ reaching a minimum value for seniority conserving transitions ($\Delta\nu = 0$). A $B(E2)$ interpretation is given within the seniority scheme and the shell-model calculations.

ACKNOWLEDGMENTS

We would like to thank the ISOLDE Collaboration and technical teams for providing the beam. C.R.N. acknowledges the insightful discussions about the β decay formalism with X. Mougeot. This work was supported through Romanian IFA Grant CERN/ISOLDE, by the Romanian Ministry of Research, Innovation and Digitization under Contract No. PN 23 21 01 02, the Spanish Funding Agency MICIN/AEI/(FEDER, EU) under Projects PID2019-104390GB-I00, PID2021-126998OB-I00, PID2022-140162NB-I00, and RTI2018-098868-B-I00, German BMBF under Contract No. 05P21PKCI1 and Verbundprojekt 05P2021, Slovak Research and Development Agency (Contract No. APVV-22-0282) and Scientific Grant Agency VEGA (Contract No. 1/0651/21), Science and Technology Facilities Council (STFC, UK) Grants No. ST/P004598/1 and No. ST/V001027/1, FWO-Vlaanderen (Belgium), C14/22/104 (BOF KU Leuven), the F.R.S.-FNRS and FWO under the Excellence of Science (EOS) Program No. 40007501, the European Research Council Grant No. 101088504 (NSHAPE) and ENSAR2: European Union's Horizon 2020 research and innovation programme under Grant Agreement No. 654002.

[1] Z. Y. Zhang *et al.*, Phys. Rev. Lett. **126**, 152502 (2021).
[2] J. Chen and F. G. Kondev, Nucl. Data Sheets **126**, 373 (2015).
[3] G. Astner, Phys. Scr. **5**, 31 (1972).
[4] G. Astner and V. Berg, Phys. Scr. **5**, 55 (1972).
[5] B. Singh, D. Abriola, C. Baglin, V. Demetriou, T. Johnson, E. McCutchan, G. Mukherjee, S. Singh, A. Sonzogni, and J. Tuli, Nucl. Data Sheets **114**, 661 (2013).
[6] R. A. Meyer, H. Kluge, K. H. Maier, A. Maj, M. Menningen, N. Roy, W. Wiegner, and M. Guttormsen, HMI-393, 86 (1983).
[7] A. Coc, C. Thibault, F. Touchard, H.T. Duong, P. Juncar, S. Liberman, J. Pinard, J. Lermé, J. L. Vialle, S. Büttgenbach, A. C. Mueller, A. Pesnelle (The ISOLDE Collaboration), Phys. Lett. B **163**, 66 (1985).
[8] D. J. Decman, H. Grawe, H. Kluge, K. H. Maier, A. Maj, N. Roy, Y. K. Agarwal, K. P. Blume, M. Guttormsen, H. Hubel, and J. Recht, Nucl. Phys. A **436**, 311 (1985).
[9] S. A. Ahmad, W. Klempt, R. Neugart, E.W. Otten, K. Wendt, C. Ekström, (The ISOLDE Collaboration), Phys. Lett. B **133**, 47 (1983).
[10] C. Lorenz, L. G. Sarmiento, D. Rudolph, D. E. Ward, M. Block, F. P. Heßberger, D. Ackermann, L.-L. Andersson, M. L. Cortés, C. Droese, M. Dworschak, M. Eibach, U. Forsberg, P. Golubev, R. Hoischen, I. Kojouharov, J. Khuyagbaatar, D. Nesterenko, I. Ragnarsson, H. Schaffner, L. Schweikhard, S. Stolze, and J. Wenzl, Phys. Rev. C **96**, 034315 (2017).
[11] K. H. Maier, Recent Spectroscopic Results in the Pb-region - Selected Topics in Nuclear Structure, in *Proceedings of XX Winter School on Physics*, edited by R. Broda, Z. Stachura, and J. Styczen (Institute of Nuclear Physics and Jagiellonian University, Zakopane, Poland, 1988), pp. 100–120.
[12] M. Guttormsen, H. Hübel, A. V. Grumbkow, Y. K. Agarwal, J. Recht, K. H. Maier, H. Kluge, A. Maj, M. Menningen, and N. Roy, Nucl. Instrum. Meth. Phys. Res. A **227**, 489 (1984).
[13] Pragati, A. Y. Deo, Z. Podolyák, P. M. Walker, A. Algora, B. Rubio, J. Agramunt, L. M. Fraile, N. Al-Dahan, N. Alkhomashi, J. A. Briz, M. E. Estevez Aguado, G. Farrelly, W. Gelletly, A. Herlert, U. Köster, and A. Maira, Phys. Rev. C **94**, 064316 (2016).
[14] K. H. Maier, T. Nail, R. K. Sheline, W. Stöffl, J. A. Becker, J. B. Carlson, R. G. Lanier, L. G. Mann, G. L. Struble, J. A. Cizewski, and B. H. Erkkila, Phys. Rev. C **27**, 1431 (1983).
[15] D. Venos, I. Adam, N. A. Bonch-Osmolovskaja, P. Caloun, K. I. Erohina, Y. I. Isakov, O. D. Kjostarova, V. A. Morozov, J. V. Norseev, and V. I. Stegajlov, J. Phys. G: Nucl. Part. Phys. **16**, 1009 (1990).
[16] H. Z. Liang, Phys. Scr. **91**, 083005 (2016).
[17] P. von Neumann-Cosel and J. N. Ginocchio, Phys. Rev. C **62**, 014308 (2000).
[18] J. N. Ginocchio and D. G. Madland, Phys. Rev. C **57**, 1167 (1998).
[19] R. Lică *et al.* (The IDS Collaboration), Phys. Rev. C **93**, 044303 (2016).
[20] ISOLDE Decay Station (IDS), isolde-ids.web.cern.ch, http://isolde-ids.web.cern.ch.
[21] M. J. G. Borge and B. Jonson, J. Phys. G: Nucl. Part. Phys. **44**, 044011 (2017).
[22] J. Chen, Nucl. Data Sheets **146**, 1 (2017).
[23] P. Kuusiniemi, F. P. Hesberger, D. Ackermann, S. Antalic, S. Hofmann, K. Nishio, B. Sulignano, I. Kojouharov, and R. Mann, Eur. Phys. J. A **30**, 551 (2006).
[24] The Lund/LBNL Nuclear Data Search, Version 2.0, S. Y. F. Chu, L.P. Ekström, and R. B. Firestone, Table of Radioactive Isotopes X-rays, http://nucleardata.nuclear.lu.se/toi/xraySearch.asp, 1999.
[25] T. Kibedi, T. W. Burrows, M. B. Trzhaskovskaya, P. M. Davidson, C. W. Nestor, Jr., Bricc v2.3s, https://bricc.anu.edu.au/, 2011.
[26] National Nuclear Data Center - Brookhaven National Laboratory, GTOL v.7.2h, https://www-nds.iaea.org/public/ensdf_pgm/, 2013.
[27] M. S. Basunia, Nucl. Data Sheets **181**, 475 (2022).
[28] M. Fisichella, A. Musumarra, F. Farinon, C. Nociforo, A. Del Zoppo, P. Figuera, M. La Cognata, M. G. Pellegriti, V. Scuderi, D. Torresi, and E. Strano, Phys. Rev. C **88**, 011303(R) (2013).
[29] National Nuclear Data Center - Brookhaven National Laboratory, LogFT, https://www.nndc.bnl.gov/logft, 2024.
[30] S. Turkat, X. Mougeot, B. Singh, and K. Zuber, At. Data Nucl. Data Tables **152**, 101584 (2023).
[31] E. Mach, R. L. Gill, and M. Moszynski, Nucl. Instrum. Meth. Phys. Res. A **280**, 49 (1989).
[32] N. Mărginean, D. L. Balabanski, D. Bucurescu, S. Lalkovski, L. Atanasova, G. Căta-Danil, I. Căta-Danil, J. M. Daugas, D. Deleanu, P. Detistov, G. Deyanova, D. Filipescu, G. Georgiev, D. Ghiţă, K. A. Gladnishki, R. Lozeva, T. Glodariu, M. Ivaşcu, S. Kisyov, C. Mihai, R. Mărginean, A. Negret, S. Pascu, D. Radulov, T. Sava, L. Stroe, G. Suliman, and N. V. Zamfir, Eur. Phys. J. A **46**, 329 (2010).
[33] M. J. Martin, Nucl. Data Sheets **114**, 1497 (2013).
[34] G. D. Dracoulis, P. M. Walker, and F.G. Kondev, Rep. Prog. Phys. **79**, 076301 (2016).
[35] B. A. Brown and W. D. M. Rae, Nucl. Data Sheets **120**, 115 (2014).
[36] E. K. Warburton and B. A. Brown, Phys. Rev. C **43**, 602 (1991).
[37] E. Caurier, G. Martinez-Pinedo, F. Nowacki, A. Poves, and A. P. Zuker, Rev. Mod. Phys. **77**, 427 (2005).
[38] E. Caurier, F. Nowacki, code NATHAN, Strasbourg, 1995.
[39] H. Naïdja, Phys. Scr. **94**, 014005 (2019).
[40] H. Naïdja, Phys. Rev. C **103**, 054303 (2021).
[41] J. J. Ressler, R. F. Casten, N. V. Zamfir, C. W. Beausang, R. B. Cakirli, H. Ai, H. Amro, M. A. Caprio, A. A. Hecht, A. Heinz, S. D. Langdown, E. A. McCutchan, D. A. Meyer, C. Plettner, P. H. Regan, M. J. S. Sciacchitano, and A. D. Yamamoto, Phys. Rev. C **69**, 034317 (2004).
[42] E. Teruya, K. Higashiyama, and N. Yoshinaga, Phys. Rev. C **93**, 064327 (2016).
[43] I. M. Govil, C. S. Khurana, Nucl. Phys. **60**, 666 (1964).
[44] W. Kratschmer, H. V. Klapdor, and E. Grosse, Nucl. Phys. A **201**, 179 (1973).
[45] I. Bergström, B. Fant, C. J. Herrlander, P. Thieberger, K. Wikstorm, and G. Astner, Phys. Lett. B **32**, 476 (1970).
[46] L. Zamick and G. Ripka, Nucl. Phys. A **116**, 234 (1968).
[47] M. Stepanov, L. Imasheva, B. Ishkhanov, and T. Tretyakova, EPJ Web Conf. **177**, 03004 (2018).
[48] L. J. Jardine, S. G. Prussin, and J. M. Hollander, Nucl. Phys. A **190**, 261 (1972).
[49] R. Firestone, *Table of Isotopes*, edited by S. F. Chu and C. Baglin (Wiley-VCH, Berlin, 1999).
[50] G. Astner, I. Bergström, J. Blomqvist, B. Fant, and K. Wikström, Nucl. Phys. A **182**, 219 (1972).
[51] M. S. M. Gerathy, A. J. Mitchell, G. J. Lane, A. E. Stuchbery, A. Akber, H. A. Alshammari, L. J. Bignell, B. J. Coombes,

J. T. H. Dowie, T. J. Gray, T. Kibédi, B. P. McCormick, L. J. McKie, M. S. Rahman, M. Reece, N. J. Spinks, B. P. E. Tee, Y. Y. Zhong, and K. Zhu, Phys. Lett. B **823**, 136738 (2021).

[52] P. Hansen, *Advances in Nuclear Physics*, edited by E. V. M. Baranger (Springer, Boston, 2004).

[53] E. Caurier, M. Rejmund, and H. Grawe, Phys. Rev. C **67**, 054310 (2003).